AIP | Review of Scientific Instruments

Facility for low-temperature spin-polarized-scanning tunneling microscopy studies of magnetic/spintronic materials prepared in situ by nitride molecular beam epitaxy

Wenzhi Lin, Andrew Foley, Khan Alam, Kangkang Wang, Yinghao Liu, Tianjiao Chen, Jeongihm Pak, and Arthur R. Smith

Citation: Review of Scientific Instruments **85**, 043702 (2014); doi: 10.1063/1.4870276
View online: http://dx.doi.org/10.1063/1.4870276
View Table of Contents: http://scitation.aip.org/content/aip/journal/rsi/85/4?ver=pdfcov
Published by the AIP Publishing

Facility for low-temperature spin-polarized-scanning tunneling microscopy studies of magnetic/spintronic materials prepared *in situ* by nitride molecular beam epitaxy

Wenzhi Lin,[a] Andrew Foley, Khan Alam, Kangkang Wang, Yinghao Liu, Tianjiao Chen, Jeongihm Pak, and Arthur R. Smith[b]
Department of Physics and Astronomy, Nanoscale and Quantum Phenomena Institute, Ohio University, Athens, Ohio 45701, USA

(Received 10 February 2014; accepted 20 March 2014; published online 8 April 2014)

Based on the interest in, as well as exciting outlook for, nitride semiconductor based structures with regard to electronic, optoelectronic, and spintronic applications, it is compelling to investigate these systems using the powerful technique of spin-polarized scanning tunneling microscopy (STM), a technique capable of achieving magnetic resolution down to the atomic scale. However, the delicate surfaces of these materials are easily corrupted by in-air transfers, making it unfeasible to study them in stand-alone ultra-high vacuum STM facilities. Therefore, we have carried out the development of a hybrid system including a nitrogen plasma assisted molecular beam epitaxy/pulsed laser epitaxy facility for sample growth combined with a low-temperature, spin-polarized scanning tunneling microscope system. The custom-designed molecular beam epitaxy growth system supports up to eight sources, including up to seven effusion cells plus a radio frequency nitrogen plasma source, for epitaxially growing a variety of materials, such as nitride semiconductors, magnetic materials, and their hetero-structures, and also incorporating *in situ* reflection high energy electron diffraction. The growth system also enables integration of pulsed laser epitaxy. The STM unit has a modular design, consisting of an upper body and a lower body. The upper body contains the coarse approach mechanism and the scanner unit, while the lower body accepts molecular beam epitaxy grown samples using compression springs and sample skis. The design of the system employs two stages of vibration isolation as well as a layer of acoustic noise isolation in order to reduce noise during STM measurements. This isolation allows the system to effectively acquire STM data in a typical lab space, which during its construction had no special and highly costly elements included, (such as isolated slabs) which would lower the environmental noise. The design further enables tip exchange and tip coating without breaking vacuum, and convenient visual access to the sample and tip inside a superconducting magnet cryostat. A sample/tip handling system is optimized for both the molecular beam epitaxy growth system and the scanning tunneling microscope system. The sample/tip handing system enables *in situ* STM studies on epitaxially grown samples, and tip exchange in the superconducting magnet cryostat. The hybrid molecular beam epitaxy and low temperature scanning tunneling microscopy system is capable of growing semiconductor-based hetero-structures with controlled accuracy down to a single atomic-layer and imaging them down to atomic resolution. © *2014 AIP Publishing LLC*. [http://dx.doi.org/10.1063/1.4870276]

I. INTRODUCTION

Understanding the critical factors that define the structural, electronic, and magnetic properties of materials remains a constant interest in condensed matter and material science research.[1,2] It becomes essential to be able to control growth with the accuracy down to the atomic layer and image with the resolution down to the atomic scale, as properties of high quality epitaxial materials are ultimately governed by their crystal structures at the atomic level.[3] Scanning tunneling microscopy (STM) enables direct imaging of material structures down to the atomic scale in real space, and investigating intrinsic electronic properties by spectroscopy measurements.[4–8] Together with characterization techniques in momentum space, such as reflection high-energy electron diffraction (RHEED), scanning tunneling microscopy, and scanning tunneling spectroscopy provide insights to structural and electronic properties. The characterization capabilities can be extended to probe local spin-dependent phenomena by using spin-polarized STM (SP-STM).[9] Hence, there has been much interest and effort toward developing STM systems and SP-STM systems in cryogenic superconducting magnetic fields.[10–20]

In terms of materials, semiconductors and semiconductor based structures play crucial roles in electronic, optoelectronic, and spintronic applications. For example, ferromagnet/semiconductor hetero-structures are used for injection of spin-polarized currents into semiconductors. Efficient spin injection has been achieved for Fe/GaAs structures.[21] Much of the outstanding properties of systems like this are

[a]Present address: Oak Ridge National Laboratory, One Bethel Valley Road, P.O. Box 2008, MS-6487, Oak Ridge, Tennessee 37831, USA.
[b]Author to whom correspondence should be addressed. Electronic mail: smitha2@ohio.edu.

determined at the surface during growth. To date, there have been many reports of intriguing magnetic and spintronic properties of nitrides and magnetically doped nitride systems, but at the same time there remain many unanswered questions about these systems. An example is transition metal-doped GaN, for example, Mn-doped GaN in which the possible magnetism of the dopant atoms has been unable to be explored directly.[22–24] Possibly even more interesting recently are reports of magnetic properties of rare earth-doped GaN systems such as Gd:GaN.[25] And of course the initial stages of magnetic layers of various types grown on semiconducting nitride surface are of high interest in the research community. Therefore, it would be highly advantageous to develop a system that is not only capable of growing high quality semiconductors, semiconductor-based structures, and magnetic layers epitaxially, but also able to investigate their structural, electronic, and even magnetic properties at high resolution. With such a system, it could be possible to address a wide range of open questions related to the possibilities of these systems for future magnetic and spintronic applications.

So therefore, we have carried out the development of a N-plasma assisted molecular beam epitaxy (PAMBE)/pulsed laser deposition facility with cryogenic superconducting magnet spin-polarized scanning tunneling microscope integrated into a UHV system. The N-plasma assisted molecular beam epitaxy growth system is designed for (although not limited to) growing nitride semiconductors and nitride semiconductor-based structures, and a wide variety of magnetic materials as well, with up to eight source ports for MBE. In addition, the growth facility also includes pulsed laser epitaxy (PLE) including up to 9 individual source targets. *In situ* STM studies on MBE- or PLE-grown samples are carried out after a sample is transferred to the analysis chamber. For developing such a system, it is necessary to properly address challenges of integrating a MBE growth system with a SP-STM system; for example, a sample handling system, which is optimized for both custom-designed N-plasma assisted MBE growth and scanning tunneling microscopy, should be employed. Integrations of modified commercial STMs to corresponding MBE facilities have been reported previously.[26–31] Another previously reported system incorporates a commercial low temperature STM (LT-STM) with a supersonic molecular beam sample preparation system.[32] In our case, we have custom-designed both the STM as well as the MBE systems and integrated them together using a modified and optimized sample handling system based on a commercial sample handling design. We have furthermore added the ability to handle the tips conveniently by integrating our tip holder system into the overall sample handling system.

The challenges associated with setting up a hybrid MBE/SP-STM system like the one described here are nontrivial, based on several competing requirements of STM and MBE. For example, it is often preferable to grow on larger sized sample holders in MBE, whereas a small sample is desirable for the STM head, first for the purpose of achieving a high-Q factor and second due to the dimensional constraints owing to the use of a split-coil superconducting magnet with limited central bore size. We have ultimately developed our system to be able to support up to a 2 in. O.D. wafer solely for MBE growth, but also to allow a 1 cm × 1 cm sample size which is carried on a relatively small-sized sample holder which can easily be inserted into the limited-space STM system.

II. INSTRUMENTS

A. Overall system layout

As illustrated in Figs. 1(a)–1(c), the system has four custom-designed chambers: (1) growth chamber (GC); (2) analysis chamber (AC); (3) central distribution chamber (CDC); and (4) load lock chamber (LLC). The GC, AC, CDC, and LLC are all interconnected chambers. All are UHV chambers except for the LLC (high vacuum), which has a viton-sealed entry door for quick loading of samples/tips into the UHV systems and only requires turbomolecular pumping (TMP). The CDC body is nearly in a cylindrical shape, with a lateral chamber diameter of 20 in. and a height of 8 in. It has a dome-shaped top. The CDC has eight ports positioned in a

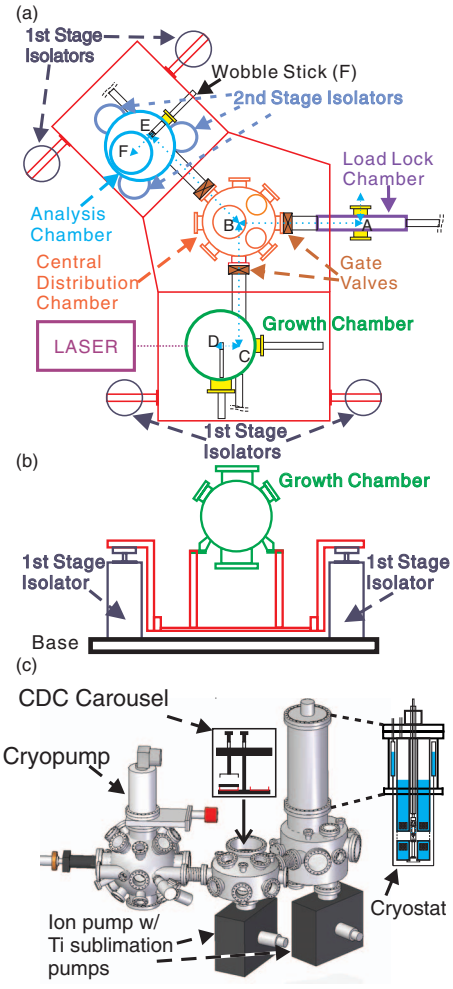

FIG. 1. Overall system layout. (a) Top view of system showing chambers and support structure. Transfer arms indicated by letters A-F; (b) illustration of table floating geometry; (c) three-dimensional (3D) model of the system. The cryostat holds the cryogenic superconducting magnet STM. Cryostat shown here without the second stage vibration isolation installed. The CDC carousel is composed of a sample transfer and storage center installed onto a 12 in. O.D. CF port of the central distribution chamber.

radial layout. Each of these ports has a 6 in. O.D. CF flange. There is a port with 12 in. O.D. CF flange at the top of the CDC for mounting a CDC carousel. Three of the eight ports of the CDC are used to join the GC, AC, and LLC via gate valves. The other five ports are for visual access or to provide expansion capabilities in the future for adding new chambers or components. The GC has a spherical chamber body of 20 in. diameter, and CF flanges of different O.D. from 2.75 in. to 10 in. The AC has a cylindrical chamber body, with a lateral chamber diameter of 20 in. and a height of 14 in. It has a 14 in. O.D. CF flange for mounting a cryostat. At the side of the AC chamber, two 8 in. O.D. CF flanges serve as view ports to enable good visual access to the STM tip and sample inside a superconducting magnet cryostat. These two view ports also provide convenient viewing when the sample/tip is transferred from the CDC to the AC using a linear transporter, and then transferred into the STM head using a wobble stick. The entire system rests on a custom-designed robust base. Four isolators are used to float the system including the base, the chambers, and the laser during STM experiments, to reduce noise transmission from the floor to the STM (Figs. 1(a) and 1(b)). The lab room that the system is located in has significant ambient noise due to air into and out of the air handling system, we have added additional damping to the entry/exit openings of the air handling system to slow down the air flow and reduce the noise.

There are ion pump (IP) and titanium sublimation pump (TSP) systems for both the CDC and AC, a cryopump (CP) for the GC (Fig. 1(c)), and a TMP backed by a scroll pump (SP) (not shown) for the LLC. As well, the TMP/SP combination, through either direct connection via the gate valve separating the LLC from the CDC or indirect connection via additional vacuum lines from the LLC to the GC and AC (not shown), can perform initial pump-downs from atmosphere, in order to reach the cross-over pressures before turning on the IPs and/or the CP. There is a vibration damper located in between the TMP and the LLC, to reduce noise transmission into the STM system during STM operation. Each of the two IPs is attached to one of two 8 in. O.D. CF flanges, which are on the bottom of both the CDC and AC. The pumping speed of each IP is 500 L/s. The single CP, which has a pumping speed of 1500 L/s, is mounted onto a 10 in. O.D. CF flange on the top of the GC.

B. Vibration and acoustic isolation

For cryogenic STM systems, particular consideration must be made for noise isolation that is not seen in room temperature STM systems. This consideration results from the desirability of rigid mechanical contact between the microscope and the cryostat in order to ensure strong thermal contact between the two. A suitable method to aid in dealing with the noise affecting such a system is to increase noise isolation between the system and the lab space containing it.[17,33]

It should be noted that this system is operated within a typical lab space, which also contains a fume hood for cleaning vacuum parts and for chemical preparations. No special elements, which would benefit STM imaging, such as isolated slabs or floating foundations, were included in the construction of the building and thus not available for the project. There is very limited means of controlling the air handling into the room. On the plus side, the room is located on the ground floor of the building. On the other hand, the lab is located in near proximity to a construction zone and thus subject to underground sonic noise disturbances. The construction projects are planned to be ongoing for the entire time the system resides in its current location. For these reasons, the system must be able to operate in a highly imperfect environment. The measures taken to limit the effect of this noise are described below.

1. 2-stage vibration isolation design

The system uses two stages of vibration isolation to protect the cryostat from mechanical noise. The first stage consists of four laminar flow vibration isolators, which float the entire roughly 2700 kg system, and is shown in Fig. 1. The second stage uses a bellows to mechanically separate the cryostat from the rest of the system.[34,35] The cryostat is then supported by three laminar flow vibration isolators. Two custom-designed double-sided conflat flanges with a cloverleaf layout were inserted and provide the support points for the three isolators. One flange provides a base for supporting the isolators, and the other a means for the isolators to lift the cryostat. The second stage vibration isolation system is shown in Fig. 2.

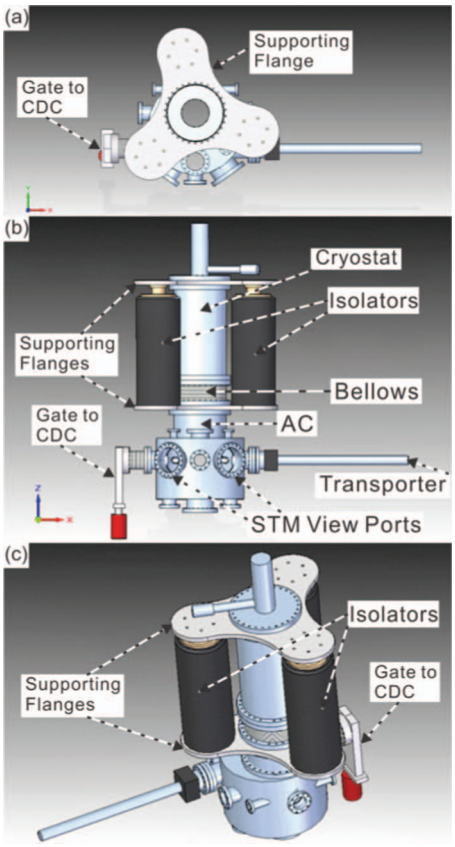

FIG. 2. Analysis chamber showing second stage of vibration isolation. Magnetic cryostat, also shown in Fig. 1, separated from rest of the chamber by bellows and supported by three laminar flow isolators. (a) Top view; (b) side view; (c) perspective view.

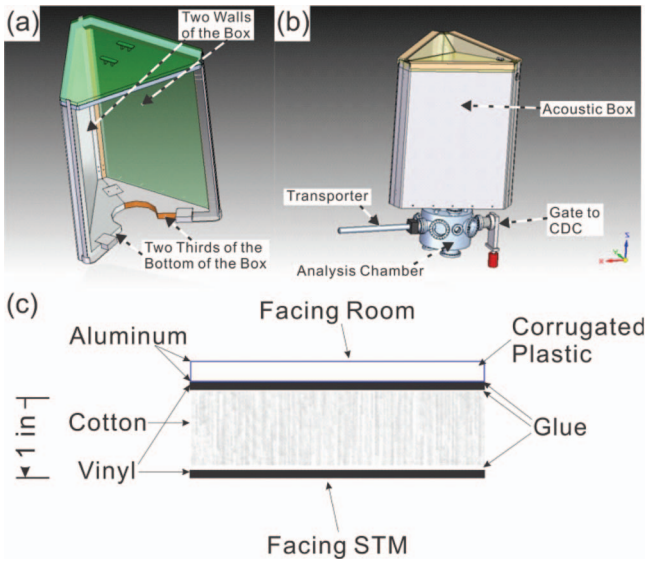

FIG. 3. Acoustic box designed to shield the STM from acoustic noise; (a) perspective view of acoustic box. The top, one side, and one third of the bottom of the box are not shown for purposes of illustration. (b) Acoustic box in position around the cryostat with the top shown as semi-transparent for purposes of illustration. Box is supported by the same flange that supports the second stage of vibration isolation shown in Fig. 2. (c) Cross-section of a wall of the acoustic box.

2. Acoustic box

The lab room that the system is located within has significant noise due to air going into and coming out of the air handling system. Therefore, we have added additional foam isolation to the entry/exit openings of the air handling system. As well, an acoustic box, which is shown in Fig. 3, is fit in place around the cryostat in order to isolate it from acoustic noise prevalent in the room. The frame of the acoustic box is attached to the same conflat flange that supports the second stage of vibration isolation. The acoustic box surrounds the cryostat with three sides, a top and a bottom, consisting of Aluminum/Plastic/Aluminum/Vinyl/Cotton/Vinyl layers sandwiched together with glue. These sound deadening walls are intended to provide additional acoustic noise shielding for the STM (Fig. 3). The acoustic box can be easily opened in order to gain access to the cryostat, and closed up during STM experiments.

C. Sample handling system

The sample handling system should meet requirements of both the N-plasma assisted MBE system and the SP-STM system. The sample holder should not only be compatible with both MBE growth experiments and SP-STM experiments, but also be able to be transferred *in situ* between the two systems. In this case, we adopted a Thermionics commercially available handling system,[36] which has the capability of handling an up to 2 in. O.D. semiconductor wafer, although smaller sample sizes are more frequently used in our experiments. In particular, for our LT-STM, the sample size is only 1 cm × 1 cm. In the following, the manner of adapting the larger sample holder "platen" system to accommodate the needs of the LT-STM is described in detail.

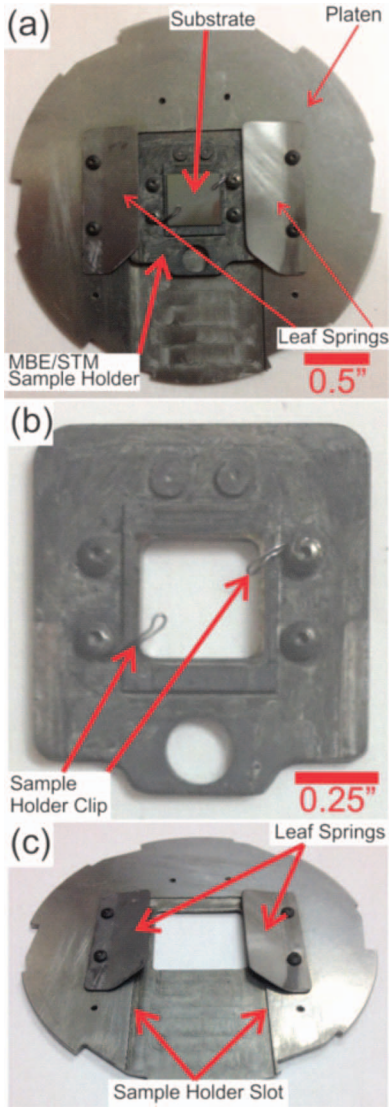

FIG. 4. MBE/STM sample holder. (a) Photograph of home-designed MBE-STM sample holder integrated onto the sample holder carrier modified from the regular MBE sample holder; (b) zoom-in view of MBE/STM sample holder; (c) perspective view of the sample holder carrier modified from the regular MBE sample holder.

The Thermionics designed sample platen is intended for MBE growth, but by itself it is not compatible with the low temperature STM. For the purpose of adapting to the low temperature STM system, the sample holder platen is modified so that it becomes a sample holder carrier (Figs. 4(a) and 4(c)) for carrying a home-designed MBE/STM sample holder (Figs. 4(a) and 4(b)). The home-designed STM sample holder is called the MBE/STM sample holder since it is compatible with, and optimized for, both STM and MBE. The MBE/STM holder is able to carry a 1 cm × 1 cm sample for both MBE and STM studies. The MBE/STM sample holder is held in the sample holder platen using leaf springs, as shown in Fig. 4(a).

The sample transfer system layout is shown in Fig. 5. By using the transfer system described above, a sample/sample holder can be loaded from atmosphere into the LLC, transferred to the CDC using transfer arm (A), by using the CDC

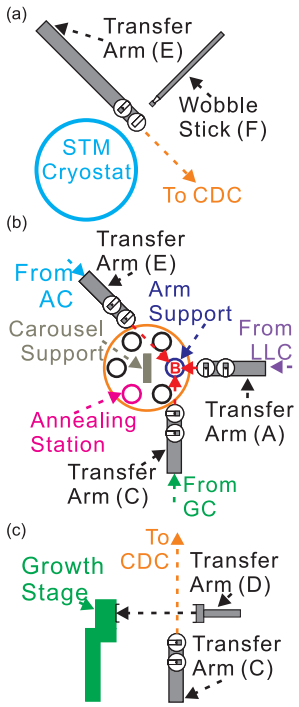

FIG. 5. Layout of sample transfer system. (a) Top view of analysis chamber transfer system; (b) top view of central distribution chamber transfer system. Red "B" denotes the location of the CDC Z-drive transporter that serves as an intermediary between horizontal transfer arms A, C, and E. An arm support provides support from beneath transfer arm A, C, or E when B picks up a platen. (c) Top view of growth chamber transfer system. Transfer arm C can rotate around its linear transfer axis in order to facilitate transfer to transfer arm D.

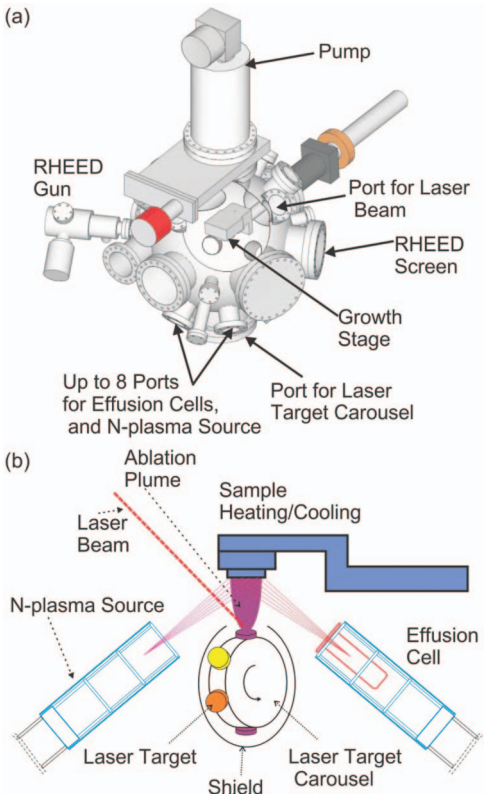

FIG. 6. N-plasma MBE/PLE growth system; (a) cut-away view of growth system; (b) illustration of the MBE and PLE source geometries with respect to the sample holder.

Z-drive transporter (B), transferred to transfer arm (D) with transfer arm (C), and finally transferred onto the growth stage. In all of this, multiple sample transfers must take place. After a fresh film is grown on the substrate, the sample/sample holder is transferred back to the CDC Z-drive transporter (B) where it can be transferred to transfer arm (E) and moved into the AC. At that point, the MBE/STM sample holder can be removed from the sample holder carrier and inserted into the STM sample stage, using a wobble stick (F).

Furthermore, the CDC is not only the sample/sample holder transfer center, but also the sample/sample holder storage center. A rotating platter can hold up to 4 sample holders at one time, any of which is accessible for use in the MBE or SP-STM. A sample is transferred first to the CDC Z-drive transporter (B) from the LLC, AC, or GC and then either stored on the platter or transferred to one of the other chambers connected to the CDC. In addition, the rotating platter also contains the sample and tip annealing station, and the tips can be coated with magnetic materials using an e-beam evaporator aimed downward toward a tip, which can be pointed upward to face the evaporator by axially rotating transfer arm (C).

D. N-plasma assisted molecular beam epitaxy growth system

The custom-designed, nitrogen PAMBE growth system is capable of growing a variety of materials with controlled accuracy down to a single mono-layer including, but not limited to, nitride semiconductors and magnetic materials. The MBE system integrates RHEED, a custom growth stage, N-plasma source, our custom-designed effusion cells, and a unique custom-built PLE system.

The epitaxial growth facility is therefore a hybrid system, containing both MBE and PLE, which may be used simultaneously or separately. The GC has totally 31 UHV ports which are used for viewports, gauges, flux sensors, effusion cells, growth stage, samples transporters, RHEED system, laser port, and future applications.

For PLE, as illustrated in the cutout view of the growth system shown in Figs. 6(a) and 6(b), the pulsed, high energy laser beam enters the laser port and impinges at an angle of ∼45° upon one of up to 9 different targets installed on a unique target carousel. The target carousel system is installed from the GC bottom port. The laser spot creates a plume, which impinges on the downward facing sample, leading to pulsed laser epitaxial growth.

For MBE, there are eight effusion cell ports, one being used for the N-plasma source, leaving 7 ports for different elemental evaporators (Fig. 6(a)). Each of the eight ports is oriented 50° away from the central vertical axis of the chamber.

MBE growth starts after setting the sample substrate to the desired sample growth temperature either by the use of the growth stage heater for high temperatures, up to ∼800-1000 °C, or in the case of low temperatures, down to −80 °C, by the use of the built-in liquid nitrogen cooling on the growth

stage. After the substrate temperature is set, one or more effusion cell shutters are opened, the elemental flux rates having been previously set to the desired values, and in the case of nitride growth, with the nitrogen plasma source active. The elemental flux rates are calibrated using an Inficon oscillating quartz crystal film thickness deposition monitor.

The *in situ* RHEED system enables monitoring of the growth in real time, a crucial capability for optimizing the growth parameters to achieve films of specified or optimized properties. The port for the 30 keV RHEED gun, and the port for an 8 in. phosphor-coated RHEED screen are both oriented 1° below the horizontal plane, at opposite sides of the chamber. The typical operating energy of the RHEED gun is 20 keV. The combination of RHEED with the sample cooling capability is also useful for investigation of surface reconstructions and surface phase changes which occur at low temperatures. Such information may be compared with LT-STM data on the same sample.

E. Cryogenic scanning tunneling microscope system and integration of MBE and STM systems

1. STM in cryogenic superconducting magnet cryostat

The commercially available cryogenic superconducting magnet cryostat (JANIS, Inc.) has a liquid nitrogen reservoir, a liquid helium reservoir, and a superconducting magnet. There is a 2.5 in. O.D. bore opening at the center of the cryostat, allowing the installation of a flow cryostat insert from the top of the helium reservoir cryostat.

The LT-STM system was designed to operate in two different configurations: (1) configured as a LT-STM (∼4.2 K) in direct contact with the base of the liquid helium reservoir cryostat; and (2) configured as a variable temperature (VT) STM in the range 4.2–300 K (by direct connection to the tip of the flow cryostat). It was chosen to first try the LT configuration since this would not require the complications of having to adjust the helium flow rate nor to be concerned about temperature stabilization as one must in a VT configuration. But in order to make it easy later to change to the VT configuration, it was decided that the electrical connections should come from the top and wind down around the flow cryostat body.

Therefore, this decision necessitated a way to support the body of the STM at the tip of the flow cryostat for insertion into the liquid helium reservoir cryostat, followed by a way to decouple the STM mechanically from the flow cryostat while at the same time being able to make a firm connection with the base of the magnet cryostat and also maintain the electrical connections coming down from the top.

Here, we describe the method of achieving these requirements. The method involved designing (1) a coupling device to be located in between the STM body and the flow cryostat in which, by a simple rotation, it is possible to either couple or decouple the STM body; and (2) a pedestal device to be located in between the STM body and the base of the magnet reservoir. These designs are shown schematically in Fig. 7.

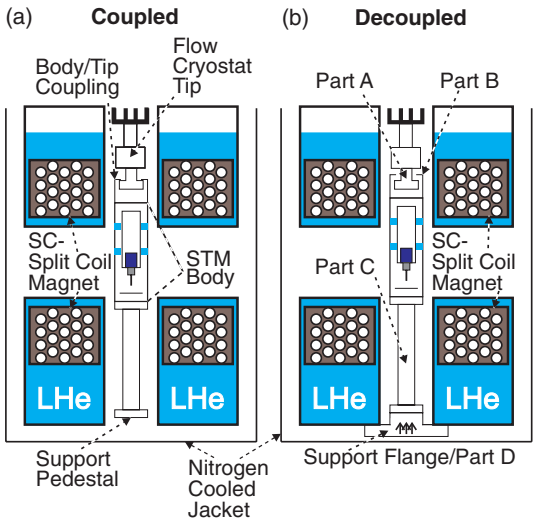

FIG. 7. Cross-sectional illustration of the installation of the STM into the cryogenic split-coil superconducting magnet cryostat; (a) STM with pedestal and coupling device on the cryostat insert supported from the top. Coupling device between tip of the flow cryostat and the STM body is interlocked. (b) STM and pedestal pushed up by the small flange and mechanically coupled to the bottom of LHe magnet cryostat. At this point, the STM body and the tip of the flow cryostat are de-coupled.

As can be seen, the coupling device consists of two parts: (1) Part A is connected to the tip of the flow cryostat by a screw; and (2) Part B is connected to the STM body by screws. Part A and Part B interlock at a certain range of angles to allow insertion of the flow cryostat into the reservoir cryostat bore (Fig. 7(a)), but at another range of angles become decoupled; at that point, it would be possible for the STM body to rise by $\sim \frac{1}{8}$ in. (at no point can it drop). There is then a position in which Part B will be physically not in contact with Part A (decoupled, see Fig. 7(b)). Whereas, the electrical connections will remain intact since the wires are designed to have some flexibility.

As can also be seen from Fig. 7, the pedestal device also consists of two parts: (1) Part C which is a long support pedestal section physically bolted to the STM body; and (2) Part D which is a small support flange to be used for bolting to the base of the flow cryostat and also to the long pedestal section. As the support pedestal is lowered into the magnet cryostat bore initially along with the STM body (Fig. 7(a)), the support flange is then connected to the pedestal by screws, pushed up slightly, rotated to decouple the coupling device at the top of the STM body, and then bolted to the base of the magnet cryostat (Fig. 7(b)). At this point, the STM should be mechanically and thermally decoupled from the flow cryostat and mechanically and thermally coupled to the magnet cryostat in the LT-STM configuration.

It should also be pointed out however, that while the support pedestal is mechanically tightened to the STM body at the bottom of the STM body via bolts and washers, it is electrically isolated from the STM body using a sapphire plate and washers painted with insulating epoxy.

The setup of the cryostat is such that a nitrogen cooled jacket, shown in Fig. 7, surrounds the superconducting magnet cryostat. This is a common method employed to

slow the boil off of the liquid helium inside an inner cryostat.[17,34,35,37,38] It should be noted that this system has the ability to freeze the nitrogen cooling the jacket by means of pumping on the liquid nitrogen reservoir using a mechanical pump located far away from the STM (in our case, the pump is located in another room across the hall from the main MBE/LT-STM room). This process is used effectively to reduce the vibrational noise from bubbling LN_2.[34,38]

2. Modular design in STM head

The microscope has been designed to be modular; it consists of an upper body and a lower body, which are attached together through three sets of bolts and nuts as seen in Fig. 8(a) (one set is not visible from the current viewing direction). The upper body is mainly for coarse approach and scanning, while the lower body is mainly for accepting a MBE-grown sample or a tip shuttle. The modular design of the STM head allows us to change the lower body easily to accommodate different sample geometries for different chamber systems/applications in the future without affecting the design of the upper body. This upper body can be conveniently adapted to fit a different MBE chamber system or even a new application beyond studying MBE-grown samples, by changing the lower body independently. To enable such a modular design, two removable bridge beams have been designed and used in the upper body. Such removable bridge beams allow the installation of 4-40 screws to attach upper body and lower body together. Furthermore, we use detachable shear piezo stack bundles, in which the shear piezo stacks for coarse approach are sitting on Macor/phosphor bronze plates. In this way, the detachable bundles can be tightened to or removed from the upper body by using 2-56 tapped holes on the upper body and 2-56 clearance holes on the plates. Such a detachable design makes it very convenient to service or modify the piezo stack bundles without affecting the main upper body. By removing the bridge beams, it is possible to conveniently tighten/loosen the detachable shear piezo stack bundles to/from the upper body.

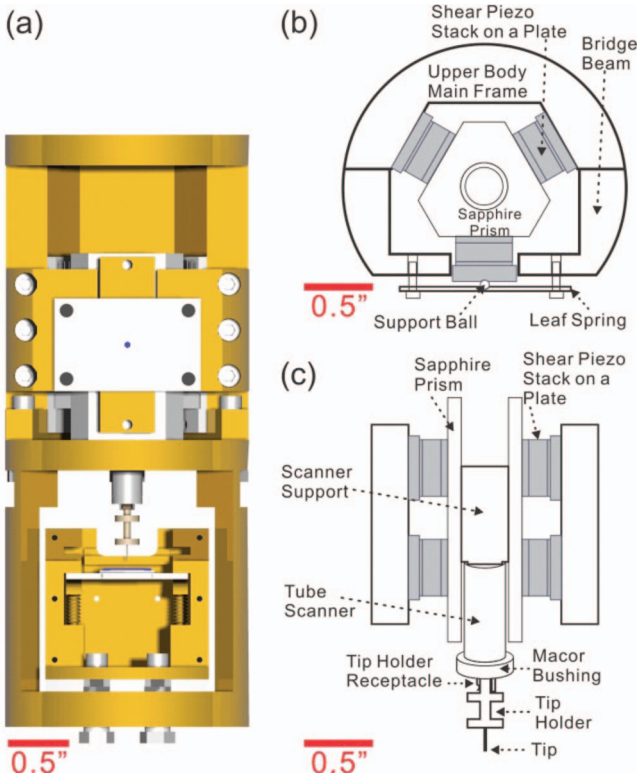

FIG. 8. (a) Modular STM design including upper and lower body; (b) top section view of upper body design; (c) side section view of upper body design showing prism and shear piezos.

Three sets of such modular designed STM heads have been built in our lab. One is successfully used in this hybrid MBE/LT-STM. The second has also been conveniently and successfully adapted to a double-stage spring suspension, room temperature STM with eddy current damping.[39] The third was built as a back-up. In this report, we will demonstrate the successful use of this modular design in a STM system at low temperature without any eddy current damping spring suspension, which is especially useful for a system containing a superconducting magnet. In such a scenario, a standard eddy current damping spring suspension system is not applicable due to interference with the superconducting magnet.

The upper body uses the well-known S.H. Pan style stick-slip inertial motor for tip coarse approach.[40] Such an approach mechanism has been used successfully in STM heads intended for spin-polarized STM studies.[13,15] One end of the scanner is glued to a Macor support, which is glued into the round inner bore of a 6-sided sapphire prism. The opposite end of the scanner supports the tip receptacle via a Macor bushing. The Macor bushing electrically separates the tip receptacle from the scanner (Fig. 8(c)). The sapphire prism is clamped by 6 sets of shear piezo stacks, with two sets applying pressure on each of 3 different sides located 120° apart. Each pair of shear piezos are attached to a plate. Two of three plates are tightened to the upper body. The third plate is pressed at its midpoint toward the sapphire prism by a small stainless steel ball, which is pushed by a molybdenum leaf spring.

3. Integration of N-plasma assisted MBE with STM

The lower body is designed to accept MBE/PLE sample holders and tip shuttles carrying tip holders. Tip holders can be loaded into the STM scanner receptacle without removing the sample holder from the sample stage. As illustrated in Fig. 9(a), the sample stage is mechanically coupled, but electrically decoupled from the lower body frame via a sapphire plate, bolts, nuts, and washers painted with insulating epoxy. The sample stage consists of three parts, which are integrated together and enable sample loading using compression springs (Figs. 9(a) and 9(b)). Screws pass through vertical holes and compression springs in parts 1 and 2 of the lower body, and then tighten into a sample ski. The holes only allow the screws to pass through, and hold compression springs against the skis. This therefore allows the sample holder to be held in place between the stationary slot surface above and the spring-loaded skis below the sample holder. The front ends of the skis are rounded to ensure smooth insertion of the

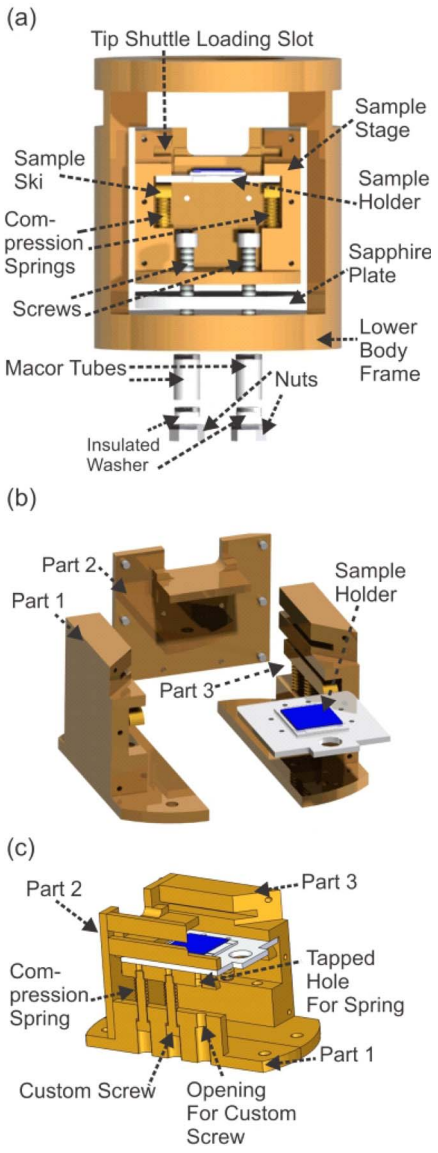

FIG. 9. Sample stage/lower body assembly. (a) Side-view of sample stage installed in the lower body; (b) sample stage disassembled into three main parts; (c) assembled sample stage with cross-section of a spring-loaded sample ski, in which one of the three springs is removed.

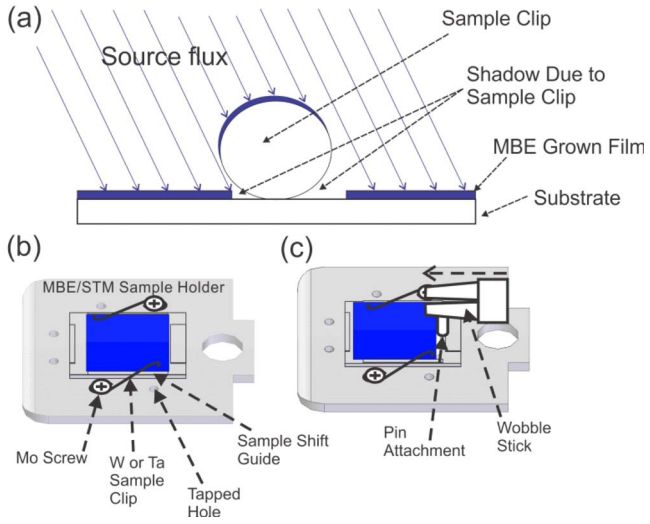

FIG. 10. (a) Illustration of shadow formed around sample clip area; (b)/(c) before/after shifting sample in sample holder using a wobble stick. Sample is guided by a slot.

sample holder into the sample stage. This design provides both flexibility for sample insertion, and stability after a sample is inserted into the STM head.

It is important to address the conductivity issues in the case of semiconductor samples, since a key purpose of the MBE/STM system is to study nitride semiconductor-based surface structures. First, it is common that nitride semiconductors are grown on insulating substrates; for instance, gallium nitride growth on sapphire substrate. Due to the high temperature of the growth, the substrate is commonly held in place using metal wire clips. These clips can also be used in STM to make the electrical contact to the sample surface. As can be seen in Fig. 10(a), however, a shadow is formed on the substrate during MBE growth in the vicinity of the sample clips. In this case, there will not be any contact between the sample clip and the freshly grown film. So if the substrate is insulating, the MBE-grown film will not have any contact to the sample bias, leading to no tunneling current. This problem will cause a tip crash during tip approach. Thus, it is essential to have a way to make contact between the sample clip and the film subsequent to growth.

One solution is to shift the sample and thus the sample/clip point of contact after the MBE growth. Figures 10(b) and 10(c) illustrate this method to achieve a good contact point between the sample and sample clip. As seen in Fig. 10(b), a wobble stick approaches the sample holder, and a small pin installed on the wobble stick pushes the sample so that the sample clip is shifted away from the shadow area on the sample surface. After this, the sample/sample holder is ready for loading into the STM sample stage.

There are separate, independent slots in the sample stage used for installing and removing STM tips without need to remove the sample. This is done via a tip shuttle (or tip holder shuttle) which carries the actual tip holder. The tip shuttle has a V-shaped opening on its top plate, allowing easy retracting of the tip shuttle after the tip/tip holder is picked up by the scanner/tip holder receptacle. The bottom plate has an open geometry to allow for annealing and magnetic coating of the tip. The lower wings of the tip shuttle, as seen in Fig. 11(a), slide into the dedicated slots on the sample stage.

A key point of the tip shuttle is to provide a means to make very good alignment of the tip holder with the tip holder receptacle attached to the scanner. If this can be achieved reliably the first time every time a tip is installed or removed from the STM, the efficiency can be very high. But it requires careful alignment in each of the two lateral (horizontal) directions. This would not be easy to do by purely a manual approach using the wobble stick, since the visual access via the telescope looking into the STM through the viewport windows, although good, is still somewhat limited. The limited visual access causes offsets to be difficult to judge. Therefore, we take an auto-alignment approach. Such an auto-alignment is achieved in this case by means of a leaf spring attached to one side of the tip shuttle and by two sets of adjustable pan

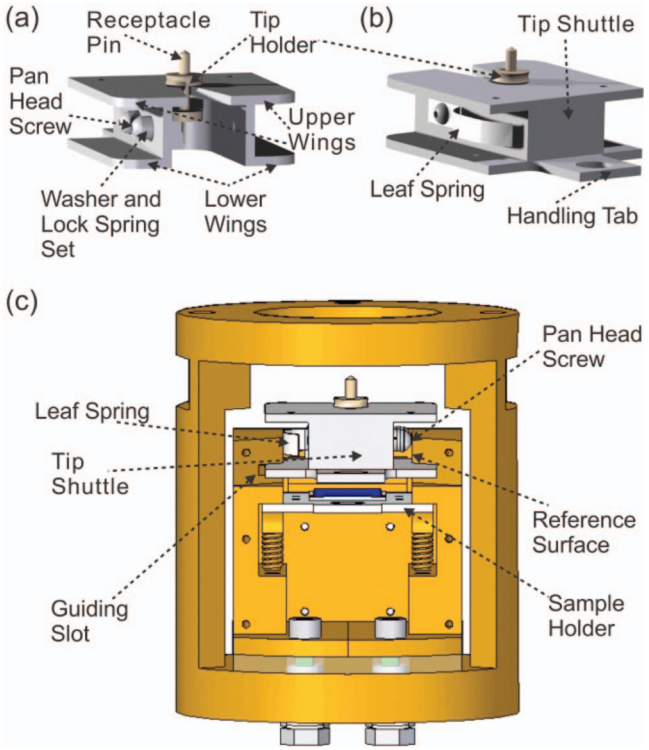

FIG. 11. Independent tip loading; (a) and (b) two views of tip shuttle with tip holder; (c) tip shuttle in tip shuttle loading slot. Sample holder does not need to be removed.

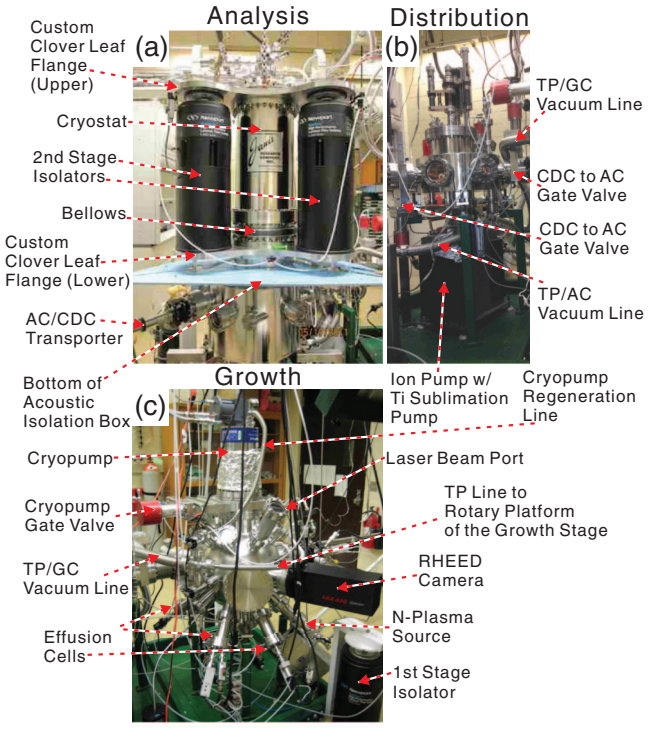

FIG. 12. System after setting up; (a) analysis system with cryogenic superconducting magnet SP-STM; (b) central distribution chamber; (c) MBE/PLE growth system.

head screws with washers and lock washers on the other side. The adjustable positions of the pan head screws determine the lateral offset position since the leaf spring on the other side forces the shuttle into the correct position. The depth position is set by pushing the tip shuttle against a stop at the back of the slot. This setup is highly successful and results in reliable and repeatable tip transfers.

III. SYSTEM START UP AND INITIAL PERFORMANCE

Figures 12 and 13 show the system after setup. The analysis system with cryogenic superconducting magnet SP-STM, the central distribution chamber, and the MBE/PLE growth system are displayed in Figs. 12(a)–12(c), respectively. In Fig. 12(b), the two gate valves, which connect the CDC to the two other UHV chambers are shown. The whole system is shown in Fig. 13.

A. Cryogenics performance

With the cryostat configured as shown in Fig. 7(b) and the flow cryostat under vacuum, the LT-STM system can be brought from room temperature to its base temperature in roughly 60 h. First, the radiation shield is cooled using LN_2. In order to save LHe, the system is initially cooled by filling the superconducting magnet dewar with LN_2 and then waiting for the LN_2 filled cryostat to cool for roughly 24 h. After this the LN_2 can be pushed out of the superconducting magnet dewar with N_2 gas. Once empty, the superconducting magnet dewar can be filled with LHe. After continuing to cool the superconducting magnet dewar and the radiation shield with LHe and LN_2, respectively, for roughly 36 h the cryostat will reach equilibrium at its base temperature.

Liquid nitrogen is used to cool a jacket surrounding the superconducting magnet cryostat, which are each shown in Fig. 7. By placing the LN_2 under vacuum, the nitrogen freezes. Freezing the LN_2 increases the typical hold time of the system by up to 4 h, from roughly 24 h to roughly 28 h. During operation at base temperature, the system consumes roughly 150 L of LHe weekly.

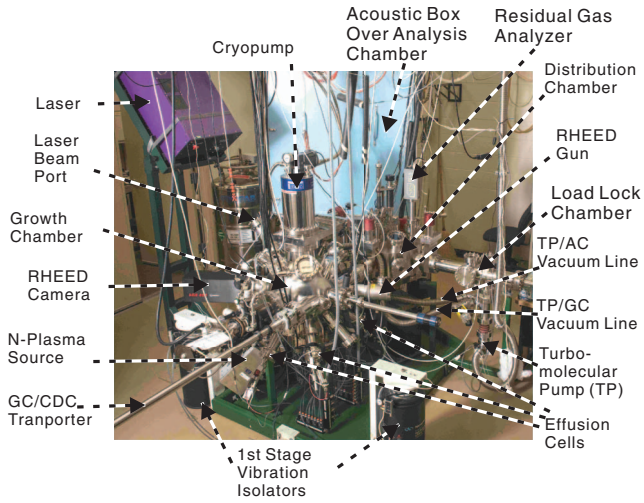

FIG. 13. View of the entire system after setting up. Includes the load-lock, growth, central distribution, and analysis chambers as well as the laser. Green base, which serves as a support for the whole system, can be lifted by the 1st stage vibration isolators.

With the system at its base temperature, the drift speed of the STM was measured by monitoring the movement of a surface defect over a period of 4 h. From this measurement, the drift speed during the 4 h was found to be a little under 3 nm/h. This amount of drift is considered to be excellent, although not as low as some LT-STM systems which have been reported.[11,14,33,34,38] The remnant drift in our system could be related to a slow asymptotic approach to the lowest base temperature. A drift speed of less than 3 nm/h is low enough that we can acquire point spectroscopy reliably on sub-nanometer scale surface defects.

B. Vibration and acoustic isolation performance

The green base, which supports the entire system, is shown in Fig. 13 with two of the four first stage vibration isolators clearly visible. The other two are installed on the far side near to the AC. These first stage isolators support the whole system, including the laser, mechanically separating it from the lab.

In Fig. 12(a), the AC is shown together with the second stage of vibration isolators installed. The second stage vibration isolators are supported by the lower custom clover leaf double sided conflat flange and support the cryostat with the upper clover leaf flange. When the isolators are pressurized, the bellows extend and contract as needed in order to maintain the vacuum seal while providing a weak connection between the cryostat and the main chamber.

The acoustic isolation box is shown fully installed on the AC system in Fig. 13. In Fig. 12(a), the acoustic box is shown with only the bottom installed. It is notable that the acoustic isolation box does not float on the second stage vibration isolators, but rather is fixed to the chamber and encloses the 14 in. OD bellows. In principle, only acoustic noise impingent on the chamber and transmitting through the bellows could be detected by the STM. Due to the mass of the whole system, this is kept to a minimum.

The middle spectrum (black) in Fig. 14 is a Fast Fourier Transform of the current noise with a STM tip approached to a c(6×12) surface reconstruction on wurtzite gallium nitride GaN(000$\bar{1}$) (tip in-range) with both stages of vibration isolators and acoustic isolation system installed and active. The amplitude of the noise stays mainly in the range of 10^{-13} A $Hz^{-1/2}$-10^{-12} A $Hz^{-1/2}$. The magnitude generally decreases with increasing frequency. It is difficult to determine the exact sources of the noise peaks in the spectrum, but certainly some of it is related to simply the stability of the tunneling junction.

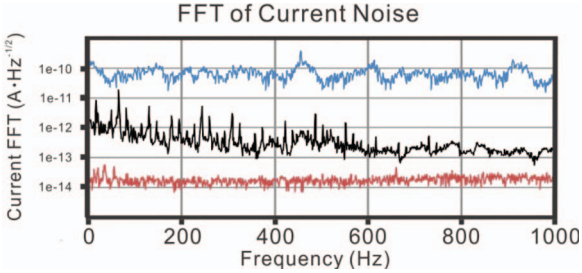

FIG. 14. Fast Fourier transform over 1 Hz intervals of the current noise on a log scale. Blue and black are while STM approached to c(6×12) reconstructions on wurtzite gallium nitride GaN(000$\bar{1}$). The nitrogen is liquid for blue and frozen for black. The tip is retracted away from the surface and nitrogen is frozen for red.

The bottom spectrum (red) was taken with the tip retracted from the surface (tip out-of-range), to provide the background noise for the system. This very flat spectrum is not sensitive to either vibrational or acoustic noise, nor to the effects of the tunneling junction. It represents the base electronic noise in the system. We see that it is in the low 10^{-14} A $Hz^{-1/2}$ level over the entire range 0–1000 Hz.

As stated previously, LN_2 is used to cool the radiation shield surrounding the superconducting magnet cryostat, which is shown in Fig. 7. It is generally known that LN_2 boils vigorously in such STM applications, leading to a broad spectrum noise. This is clearly seen in the top spectrum (blue) of Fig. 14; this spectrum was acquired under such LN_2 boiling conditions and is generally 2-3 orders of magnitude worse compared to the middle (black) spectrum which was acquired after freezing the LN_2 to become solid N_2. Certainly, it is highly advantageous for vibration isolation to freeze the LN_2, not to mention the benefit of the increased hold time.

C. Pumping and vacuum performance

The TMP backed by the SP can complete the initial pump down from atmosphere in order to reach the cross-over pressures needed by the CP and two IPs, which pump the GC, AC, and CDC, respectively, as well as the LLC. The TMP is directly connected to the LLC and so pumping the LLC is the most efficient. The CDC is connected directly to the LLC through a 6 in. gate valve and is therefore pumped easily through the LLC. The AC and GC are directly connected to the LLC through two large-ID, flexible bellows vacuum pumping lines, which connect to the TMP directly and are valved off using a series of smaller gate valves; these pumping lines are shown in Figs. 13 and 12. With this setup, it is possible to separately and independently pump down or ventilate any of the 4 chambers. During initial pump down by the TMP, the pressure in the AC, GC, or CDC can be brought from atmosphere down to about 5×10^{-6} Torr. Once the respective main pump (cryopump or ion pump) is turned on, base pressures below 2×10^{-10} Torr are easily reached. For the AC system, the pressure drops into the 10^{-11}'s during cryogenic cooling, and for the GC, the base pressure improves after each subsequent nitride film growth, which also provides a fresh gettering layer for the GC.

A freshly grown sample can be transferred from the GC to the CDC and then on to the AC, where it is then transferred to the LT-STM using the wobble stick. During the transfer from GC to CDC to AC and finally into the LT-STM, the steady state vacuum pressure seen by the sample does not exceed 2×10^{-10} Torr. Such vacuum levels are sufficient to ensure that the rate of adsorption of contaminants onto a freshly grown sample surface is low enough to keep the surface clean for STM measurements for more than 3 days. For example, surface adsorbate densities will remain small enough to allow wide clean areas of surface reconstruction to be visible.

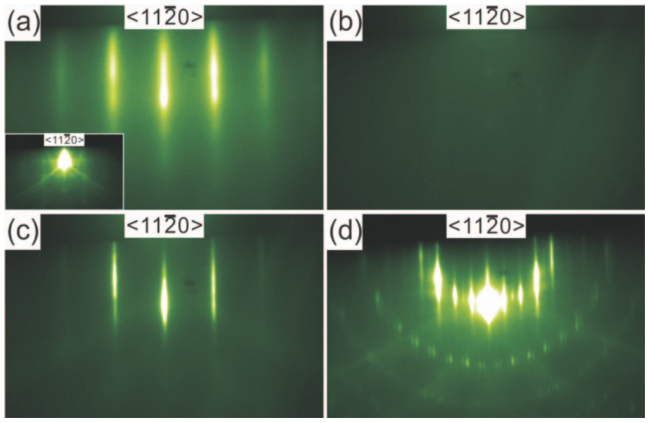

FIG. 15. Real-time RHEED patterns of wurtzite GaN(000$\bar{1}$) growth on sapphire, taken along $\langle 11\bar{2}0\rangle$; (a) sapphire substrate annealed with N-plasma at a high temperature. Inset is the sapphire substrate before annealing; (b) initial stage of the low temperature GaN buffer layer; (c) at higher temperature after the growth of the low temperature GaN buffer layer; (d) smooth GaN surface cooled toward room temperature.

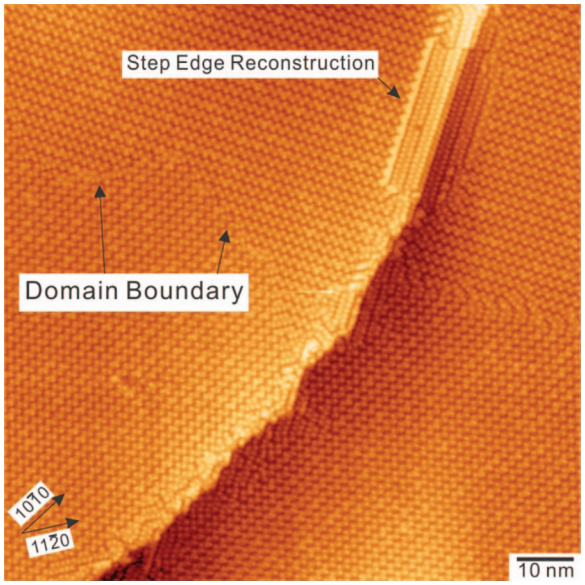

FIG. 16. STM image of c(6×12) reconstructions on wurtzite gallium nitride GaN(000$\bar{1}$), $V_s = +1.00$ V, $I_t = 0.1$ nA, the system is cooled with LHe.

D. Results

To demonstrate the successful operation of the system, we carried out a MBE/LT-STM experiment involving GaN. Figure 15 shows the real-time *in situ* RHEED monitoring of the growth of a Ga-rich GaN(000$\bar{1}$) film on sapphire, taken along $\langle 11\bar{2}0\rangle$. We chose this as a starting sample for several reasons: (1) the Ga-rich surface is metallic/highly conductive; (2) the higher-order reconstructions are easy to obtain by MBE growth; and (3) much is known about these N-polar GaN reconstructions. Ga-rich GaN surfaces have been studied using RHEED and STM by Smith *et al.*[41] previously. Therefore, they can be used for x-y scanner calibration, and the abundance of steps can be used for z-calibration. The inset of Fig. 15(a) shows a RHEED pattern of the sapphire substrate before GaN growth, also taken along $\langle 11\bar{2}0\rangle$. The surface quality significantly improves after high temperature ($T = 700\,^{\circ}$C) N-plasma annealing, as suggested by the streaky RHEED pattern in Fig. 15(a). The RHEED pattern shown in Fig. 15(b) demonstrates the initial nucleation phase of the low temperature ($T = 620\,^{\circ}$C) GaN buffer layer. The streaky RHEED pattern in Fig. 15(c), taken at $T = 700\,^{\circ}$C, indicates formation of a high-quality, low temperature GaN buffer layer. Subsequent high temperature ($T = 700\,^{\circ}$C) growth of GaN results in a smooth Ga-rich GaN surface. After cooling the high-quality grown surface to temperatures below $\sim$300 °C and down to room temperature, the reconstruction streaks appear, and these are seen clearly in the RHEED pattern taken at $T = 80\,^{\circ}$C, shown in Fig. 15(d). There we see clearly the first zone 3× streaks as well as slightly weaker first zone 6× streaks. The second zone shows the short streak doublets having also 3× spacing, centered at the $\frac{1}{6}$th, $\frac{3}{6}$th, and $\frac{5}{6}$th positions. This RHEED pattern is characteristic of the c(6×12) reconstruction, one of 4 main reconstructions of this surface.

Figure 16 shows the atomic resolution STM image of the *in situ* grown GaN c(6×12) surface. The size of this image is ~ 100 nm × 100 nm. Epitaxially smooth terraces on GaN and atomically resolved c(6×12) reconstructions consisting of an arrangement of Ga adatoms are clearly visible in the image. The Ga adatoms are arranged into pairs, and these pairs repeat along parallel rows, with the pairs at an angle of $\sim 30^{\circ}$ to the rows. Distinct domain boundaries are easily revealed. The domains at two sides of the boundary have orientations that are 120° away from each other, as expected for GaN, having threefold symmetry. It is also possible to observe brilliant step-edge structures all along the step edges. And, as clearly the image quality is very high, it is possible to observe even finer scale features of the c(6×12) reconstruction compared to what has been previously published for this surface, especially as the voltage bias is varied.

Figure 17(a) shows a further zoomed-in image of the N-polar GaN c(6×12) surface, and height profiles along two lines are shown in Figs. 17(b) and 17(c). Along the high angle line (green), which is orthogonal to the c(6×12) rows and closest to the slow scan direction, the corrugation is measured to be $\sim$0.10 nm (1.0 Å); the noise level is observed as variations from the ideal corrugation line of $\sim$0.01-0.02 nm (0.1-0.2 Å). Along the fast scan direction (blue line), the overall corrugation amplitude is measured as $\sim$0.11 nm (1.1 Å); the noise level is more difficult to measure here, but less than $\sim$0.01 nm (0.1 Å). Certainly, the corrugations on this surface are large, but the noise levels are very low, leading to the very high image quality.

IV. SUMMARY

We have carried out the development of a nitride MBE/PLE growth system combined with a cryogenic superconducting magnet spin-polarized scanning tunneling microscope system. The system is designed for the explicit purpose of investigating magnetic and spintronic material systems, but can of course be also used for more general purposes. Integrated into a home-designed UHV multi-chamber system, the

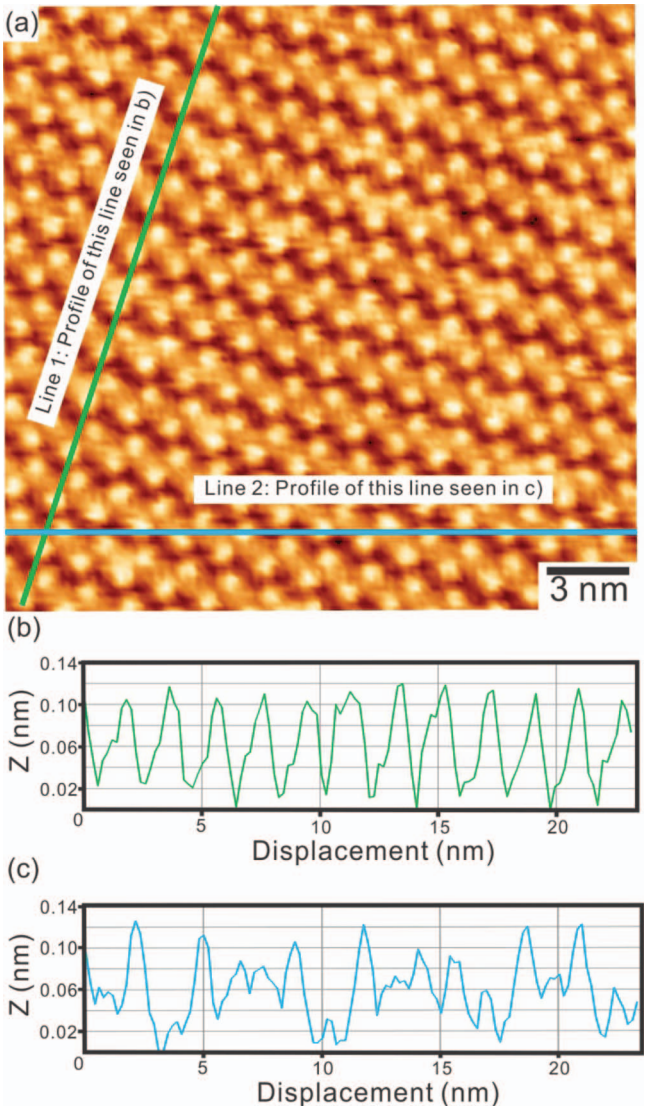

FIG. 17. (a) Raw data of a zoomed-in region within Fig. 16; (b) height profile of line 1 drawn on (a); (c) height profile of line 2 drawn on (a). This line corresponds to the direction of the scan.

MBE/PLE growth system supports up to eight MBE sources, including seven effusion cells and a N-plasma source. The PLE system allows for up to 9 pulsed laser targets, multiplying the variety of samples which may be investigated.

The LT-STM system is built into a superconducting magnet cryostat and may be operated as a low-T system as shown here, or as a variable temperature system in the future. The microscope allows for *in situ* sample and tip exchanges without breaking vacuum or even warming up the cryostat. The sample/tip handling system is optimized for both the MBE/PLE growth system and for the LT-STM system. As such, both the MBE/PLE and STM systems are integrated into a single functional hybrid system. The system successfully integrates an *in situ* MBE growth system with a low temperature STM using the sample/tip handling system. The system is capable of growing samples with controlled accuracy down to the single atomic level. A central distribution chamber allows for sample storage as well as tip annealing and magnetic tip coating, besides acting as the distribution center for samples and tips. We have demonstrated successful atomic-scale imaging of the GaN c(6×12) surface at LHe temperature. The noise levels observed in the LT-STM system are low enough to allow for the acquisition of high quality STM data.

ACKNOWLEDGMENTS

This facility was initially funded by a U.S. Office of Naval Research (ONR) DURIP grant, under Award # N00014-05-1-0418 (major equipment components, including UHV chambers, helium cryostat, HV and UHV pumps, valves, gauges, controllers, MBE growth stage, RHEED system, and rf N-plasma source), with subsequent support by the (U.S.) Department of Energy (DOE), Office of Basic Energy Sciences, Division of Materials Sciences and Engineering, under Award # DE-FG02-06ER46317 (general setup, testing, and operation of the system). Additional related support is acknowledged from the National Science Foundation (NSF), under Award # 0730257 (design and setup specific to cryogenic and vibration isolation features of the system). The authors would also like to thank Mr. Doug Shafer, Mr. Jeremy Dennison, and Mr. Michael Myers for machining many components of the system in the machine shop, and Mr. Todd Koren for electronics support. Alan Savage, Soo-Hyun Hwang, and Joseph Corbett are acknowledged for their work on effusion cell construction. Daniel Bergman, Milo Swinkels, and Abhijit Chinchore are acknowledged for their work on the PLE system.

[1]F. Marczinowski, J. Wiebe, J.-M. Tang, M. E. Flatté, F. Meier, M. Morgenstern, and R. Wiesendanger, Phys. Rev. Lett. **99**, 157202 (2007).
[2]B. Lukanov, K. Garrity, S. Ismail-Beigi, and E. I. Altman, Phys. Rev. B **85**, 195316 (2012).
[3]M. Sowwan, Y. Yacoby, J. Pitney, R. MacHarrie, M. Hong, J. Cross, D. Walko, R. Clarke, R. Pindak, and E. Stern, Phys. Rev. B **66**, 205311 (2002).
[4]L. Meng, Y. Wang, L. Zhang, S. Du, R. Wu, L. Li, Y. Zhang, G. Li, H. Zhou, W. A. Hofer, and H.-J. Gao, Nano Lett. **13**, 685 (2013).
[5]J. M. LeBeau, Q. O. Hu, C. J. Palmstrøm, and S. Stemmer, Appl. Phys. Lett. **93**, 121909 (2008).
[6]C.-L. Song, Y.-L. Wang, P. Cheng, Y.-P. Jiang, W. Li, T. Zhang, Z. Li, K. He, L. Wang, J.-F. Jia, H.-H. Hung, C. Wu, X. Ma, X. Chen, and Q.-K. Xue, Science **332**, 1410 (2011).
[7]J. M. P. Martirez, E. H. Morales, W. A. Saidi, D. A. Bonnell, and A. M. Rappe, Phys. Rev. Lett. **109**, 256802 (2012).
[8]A. Richardella, P. Roushan, S. Mack, B. Zhou, D. A. Huse, D. D. Awschalom, and A. Yazdani, Science **327**, 665 (2010).
[9]R. Wiesendanger, H.-J. Güntherodt, G. Güntherodt, R. J. Gambino, and R. Ruf, Phys. Rev. Lett. **65**, 247 (1990).
[10]J. Ferris, J. Kushmerick, J. Johnson, M. Youngquist, R. Kessinger, H. Kingsbury, and P. Weiss, Rev. Sci. Instrum. **69**, 2691 (1998).
[11]B. Stipe, M. Rezaei, and W. Ho, Rev. Sci. Instrum. **70**, 137 (1999).
[12]E. Foley, A. Kam, and J. Lyding, Rev. Sci. Instrum. **71**, 3428 (2000).
[13]O. Pietzsch, A. Kubetzka, D. Haude, M. Bode, and R. Wiesendanger, Rev. Sci. Instrum. **71**, 424 (2000).
[14]T. Mashoff, M. Pratzer, and M. Morgenstern, Rev. Sci. Instrum. **80**, 053702 (2009).
[15]S. Meckler, M. Gyamfi, O. Pietzsch, and R. Wiesendanger, Rev. Sci. Instrum. **80**, 023708 (2009).
[16]M. Dreyer, J. Lee, H. Wang, and B. Barker, Rev. Sci. Instrum. **81**, 053703 (2010).
[17]Y. J. Song, A. F. Otte, V. Shvarts, Z. Y. Zhao, Y. Kuk, S. R. Blankenship, A. Band, F. M. Hess, and J. A. Stroscio, Rev. Sci. Instrum. **81**, 121101 (2010).
[18]S. H. Kim and A. de Lozanne, Rev. Sci. Instrum. **83**, 103701 (2012).
[19]S. Misra, B. B. Zhou, I. K. Drozdov, J. Seo, L. Urban, A. Gyenis, S. C. J. Kingsley, H. Jones, and A. Yazdani, Rev. Sci. Instrum. **84**, 103903 (2013).

[20]U. R. Singh, M. Enayat, S. C. White, and P. Wahl, Rev. Sci. Instrum. **84**, 013708 (2013).
[21]A. T. Hanbicki, B. T. Jonker, G. Itskos, G. Kioseoglou, and A. Petrou, Appl. Phys. Lett. **80**, 1240 (2002).
[22]M. L. Reed, N. A. El-Masry, H. H. Stadelmaier, M. K. Ritums, M. J. Reed, C. A. Parker, J. C. Roberts, and S. M. Bedair, Appl. Phys. Lett. **79**, 3473 (2001).
[23]T. Sasaki, S. Sonoda, Y. Yamamoto, K. Suga, S. Shimizu, K. Kindo, and H. Hori, J. Appl. Phys. **91**, 7911 (2002).
[24]B. Sanyal, O. Bengone, and S. Mirbt, Phys. Rev. B **68**, 205210 (2003).
[25]S. Dhar, O. Brandt, M. Ramsteiner, V. F. Sapega, and K. H. Ploog, Phys. Rev. Lett. **94**, 037205 (2005).
[26]M. Tanimoto, J. Osaka, T. Takigami, S. Hirono, and K. Kanisawa, Ultramicroscopy **42–44**, 1275 (1992).
[27]L. J. Whitman, P. M. Thibado, F. Linker, and J. Patrin, J. Vac. Sci. Technol. B **14**, 1870 (1996).
[28]J. B. Smathers, D. W. Bullock, Z. Ding, G. J. Salamo, P. M. Thibado, B. Gerace, and W. Wirth, J. Vac. Sci. Technol. B **16**, 3112 (1998).
[29]S. Vèzian, Ph.D. thesis, Universitè de Nice Sophia Antipolis, 2000.
[30]K. Lüdge, B. D. Schultz, P. Vogt, M. M. R. Evans, W. Braun, C. J. Palmstrøm, W. Richter, and N. Esser, J. Vac. Sci. Technol. B **20**, 1591 (2002).
[31]J. K. Kawasaki, R. Timm, T. E. Buehl, E. Lundgren, A. Mikkelsen, A. C. Gossard, and C. J. Palmstrøm, J. Vac. Sci. Technol. B **29**, 03C104 (2011).
[32]M. Smerieri, R. Reichelt, L. Savio, L. Vattuone, and M. Rocca, Rev. Sci. Instrum. **83**, 093703 (2012).
[33]H. Zhang, U. Memmert, R. Houbertz, and U. Hartmann, Rev. Sci. Instrum. **72**, 2613 (2001).
[34]R. Gaisch, J. K. Gimzewski, B. Reihl, R. R. Schlittler, M. Tschudy, and W. D. Schneider, Ultramicroscopy **42–44**, 1621 (1992).
[35]R. R. Schulz and C. Rossel, Physica B **194–196**, 389 (1994).
[36]Available from Thermionics. Sample Exchange System, Patent 5,705,128 (6 January 1998).
[37]H. Okamoto, and D. Chen, Rev. Sci. Instrum. **72**, 1510 (2001).
[38]L. Zhang, T. Miyamachi, T. Tomani, R. Dehm, and W. Wulfhekel, Rev. Sci. Instrum. **82**, 103702 (2011).
[39]K. Wang, W. Lin, A. V. Chinchore, Y. Liu, and A. R. Smith, Rev. Sci. Instrum. **82**, 053703 (2011).
[40]S. H. Pan, E. W. Hudson, and J. C. Davis, Rev. Sci. Instrum. **70**, 1459 (1999).
[41]A. R. Smith, R. M. Feenstra, D. W. Greve, M. S. Shin, M. Skowronski, J. Neugebauer, and J. E. Northrup, J. Vac. Sci. Technol. B **16**, 2242 (1998).